A Parametric Study of GFRP Composite Beams with Encased I-Section using 3D Finite Element Modeling

Fahad M. Bahlol
Department of Civil Engineering, University of Baghdad, Iraq
fahad.abdulkarim2001d@coeng.uobaghdad.edu.iq (corresponding author)

Ali Hussein Ali Al-Ahmed
Department of Civil Engineering University of Baghdad, Iraq
dr.ali-alahmed@coeng.uobaghdad.edu.iq

Received: 1 October 2024 | Revised: 22 October 2024 and 31 October 2024 | Accepted: 18 November 2024

 DOI: https://doi.org/10.48084/etasr.9149

ABSTRACT

Glass Fiber Reinforced Polymer (GFRP) materials play a crucial role in the construction industry due to their lightweight properties, corrosion resistance, and high strength. Furthermore, the GFRP reinforcement ratio is a significant factor in the strength design philosophy that governs the design of flexible members. This study presents a parametric investigation of the performance of concrete composite beams reinforced and encased with pultruded GFRP. This study investigates the effect of concrete compressive strength and GFRP reinforcement ratio on the structural behavior of composite beams with encased GFRP sections under static loads. To achieve this objective, five simply supported models were numerically simulated using the Abaqus software. The reference model comprised normal concrete with a 30 MPa compressive strength, 0.42% GFRP longitudinal reinforcing ratio, and transverse steel rebars, with the GFRP I-section encased in the center of the cross-section. The other models maintained similar properties and geometries but varied in reinforcement ratio (0.85% and 1.2%) and compressive strength (25 MPa and 20 MPa). The results showed that increasing the reinforcement ratio in composite beams with encased GFRP sections improved the ultimate capacity by approximately 29% and 41% for 0.85% and 1.2% ratios, respectively, compared to the reference beam. Conversely, reducing compressive strength below 30 MPa decreased maximum load by about 16% and 23% for 25 MPa and 20 MPa values, respectively, in relation to the reference beam.

Keywords-pultruded GFRP; Abaqus CAE/2019; GFRP reinforcement ratio; flexural members

I. INTRODUCTION

GFRP composite materials provide great advantages for harsh environmental conditions. Conversely, the corrosion of steel reinforcing bars causes significant deterioration of concrete structures, resulting in cracks, spalling of the concrete cover, and a reduced load-bearing capacity [1, 2]. Accordingly, composite beams with encased GFRP materials offer corrosion resistance, electromagnetic neutrality, high strength-to-weight ratios, and high tensile strength, making them a popular choice in the construction sector as a viable alternative to steel [3-5]. The drawbacks of GFRP reinforcement include: 1) a lower elastic modulus compared to steel, 2) limited ductility (linear-elastic until failure), 3) an ineffective force transfer mechanism (bond system) with the surrounding concrete, 4) concerns regarding serviceability (increased crack width and deflections), and 5) a higher initial cost compared to steel reinforcing bars [6-8]. Experimentally, encasing a GFRP beam with concrete increases its maximum load and flexibility [9]. Currently, structural parts with high strength and low weight are crucial for modern construction [10, 11]. Concrete composite sections are commonly designed to ensure tension-controlled behavior, but the non-ductile behavior of GFRP materials supports the reconsideration of this methodology [12, 13]. Therefore, this study was based on a compression-controlled approach for encased GFRP composite beams. The main goals of this parametric study are to study the effect of the reinforcement ratio on the flexural performance of reinforced concrete composite beams with encased GFRP I-sections under static loads and numerically investigate the efficacy of decreasing the compressive strength on the failure mode, ultimate capacity, and deformation response.

II. METHOLODOLOGY

The methodology adopted in this research involved parametric numerical analysis, which is part of a wider research effort carried out at the University of Baghdad, College of Engineering. The analytical models under consideration

consisted of five concrete composite beams with encased GFRP I-sections subjected to a two-point static load. The beam had a compressive strength of 30 MPa and was designed with a cross-section of 350 mm ×200 mm, overall length of 3000 mm, clear span of 2700 mm, and shear span of 900 mm, following the recommendations described in [14]. Steel stirrups with a diameter of 8 mm and a spacing of 200 mm provided transverse reinforcement according to [15]. The longitudinal and transverse reinforcing bars were used according to the ACI 440.2R-15 [13]. The flexural reinforcement comprises five GFRP rebars with a diameter of 8 mm, two in the compression zone and three in the tensile zone to prevent flexural failure and premature shear failure [16, 17]. Figure 1 shows the geometry of the numerical models.

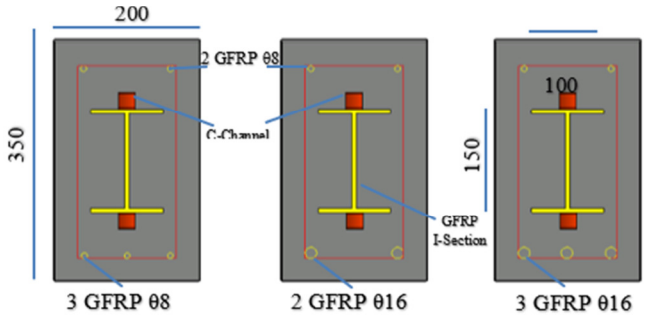

Fig. 1. Geometry of models a) B1, b) B2, and c) B3.

All models had C-channel connectors instilled on the upper and lower extreme surfaces of the pultruded GFRP I-section according to [18, 19]. The reference composite beam with the encased GFRP I-section is labeled as B1, which has an FRP reinforcement ratio (ρ_f) of 0.42%. The beams B2 and B3 have reinforcement ratios ρ_f=0.85 and ρ_f=1.2%, respectively, according to [20]. The compressive strength was 30 MPa for the three models, based on [15]. Models B4 and B5 had the same geometry as the reference, but with compressive strengths of 25 and 20 MPa, respectively, as illustrated in Table I.

TABLE I. MAIN CHARACTERISTICS OF BEAM MODELS

No	Group	Model	Compressive strength (MPa)	Reinforcement ratio
1	Ref	B1	30	0.42
2	I	B2	30	0.85
3		B3	30	1.2
4	II	B4	25	0.42
5		B5	20	0.42

III. MATERIALS DETAILS

The composite beam with the encased GFRP I-section was assembled at the center of the cross-section, and for reference model B1, five 8-mm GFRP rebars for longitudinal reinforcement were also added. Although the stirrups were made of steel with a diameter of 8 mm, they had a nominal tensile strength of 550 MPa. All the stirrups were positioned at a spacing of 200 mm through the total length. Additionally, to enhance the connection interface between the GFRP beam and concrete in the compression and tension zones, steel c-channel connectors with dimensions of 75, 50, and 3 mm were inserted. The current study specified a minimum number of channels with 30 parts and a longitudinal spacing of 200 mm, with 15 channels for each surface. All the above limitations were selected according to [13, 14, 18]. Tables II-V list the characteristics of the materials used.

TABLE II. MECHANICAL PROPERTIES OF GFRP BEAMS

Mechanical Properties	Value (MPa)
Transverse compressive strength	336
Longitudinal compressive strength	305
Longitudinal tensile strength	347
Longitudinal modulus of elasticity	38500
Transverse modules of elasticity	32200

TABLE III. TENSILE PROPERTIES OF GFRP BARS

Bar diameter (mm)	Measured area (mm^2)	Ultimate stress (MPa)	Modulus of elasticity (GPa)	Ultimate load (kN)
8	50.27	1215	55	61

TABLE IV. TENSILE PROPERTIES OF STEEL STIRRUPS

Bar diameter (mm)	Measured diameter (mm)	Yield stress (MPa)	Ultimate stress (MPa)	Modulus of elasticity (GPa)
8	7.79	465	598	210

TABLE V. MATERIAL PROPERTIES OF C-CHANNEL CONNECTORS

Yield strength (MPa)	Tensile strength (MPa)	Elongation
346	427	36%

IV. MODELING

Five composite specimens were modeled using the Abaqus commercial software version of 2019 [21]. The properties of the materials were identified, and the parts were assembled to create a complete model, as displayed in Figure 2. Six parts were simulated using various types of elements: C3D8R type for concrete, adhesive, and shear connectors, T3D2 type for steel and GFRP reinforcement, and S8R type for GFRP I-section. The numerical boundary conditions for the static FEA were adopted as a simply supported beam. The first supports were restrained in the Y and Z directions, representing the hinged support. Simultaneously, the second support was restrained only in the Y-direction, which expresses the roller support, and the entire model allows rotations in the X-direction [22]. The boundary conditions and loads were defined and subjected to two concentrated loads applied at the third point, with a clear span of 2700 mm. A mesh module was used to represent the load-displacement behavior of the beam models [23]. Different mesh size, 80, 60, and 40 mm, were used to characterize the mesh sensitivity of the simulations [24, 25].

Thus, the present study was conducted on simply supported beams using a displacement loading procedure [26, 27]. The loads at the two points increased gradually at a rate of 5

kN/min [28, 29]. Eventually, the outcome table was organized to measure the vertical mid-span deflections and ultimate load capacity of the beam models to evaluate the structural performance of the proposed models in this parametric study.

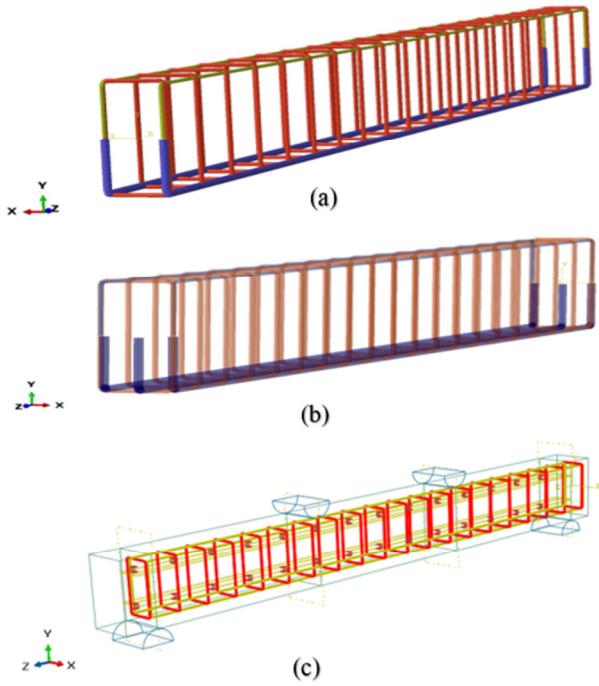

Fig. 2. Simulation of models with a) ρ_f=0.85%, b) ρ_f=1.2%, and c) ρ_f=0.42%.

V. RESULTS

This section includes the effect of the two parameters on the ultimate capacity, mid-span deflection at service, and maximum load stages of the beam models.

A. Effect of GFRP Longitudinal Reinforcement Ratio

Three ratios, 0.42%, 0.85%, and 1.2%, were used in this study to explain the effect of increasing the GFRP reinforcement ratio (ρ_f). The current study represents the first ratio by submitting five rebars with diameters of 8 mm, three in the tension region and two in the compression region. The other reinforcing ratio was submitted with a diameter of 16 mm in the tension zone for a ρ_f of 0.85 and 1.2%. Two GFRP rebars for ρ_f = 0.85% and three for ρ_f = 1.2% are displayed in Figure 2. Table VI lists all these analytical results, and Figure 3 explains the relationship between the load and the corresponding deflection at the mid-span.

TABLE VI. THE EFFECT OF REINFORCEMENT RATIO

ρ_f (%)	Max. load (kN)	Increasing max. load (%)	Def. at service load (mm)	Dec. def. at service load (%)	Max def.	Inc. max. def. (%)
0.42	146	-	29	-	45	-
0.85	188	29	24	17.24	52	15
1.2	206	41	25	13.79	55	22

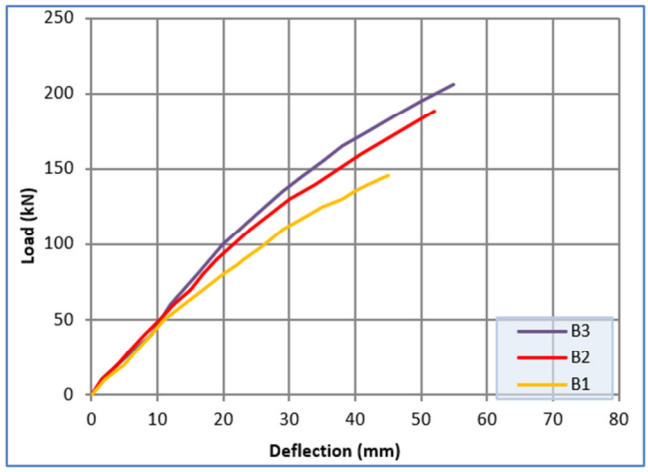

Fig. 3. Load-deflection curves of models with different reinforcement ratios.

Briefly, the above curves prove the significant effect of increasing the reinforcing ratio on the analyzed models on the ultimate capacity and deflections at the service and maximum stages. The general action was linear until the concrete crushing returned to the controlling limit state for concrete crushing/the latter, as demonstrated in Figure 3. The maximum load for the B1 model was enhanced by approximately 29% and 41% for the reinforcing ratios of 0.85% and 1.2%, respectively. However, the same results ensured a decrease in the deflection at the service stage and an increase at the maximum stage. Specifically, the decrease in deflection was approximately 17.24% and 13.79% at the service stage and 15% and 22% at the maximum load stage for models with ratios of 0.85 and 1.2%, respectively.

B. Effect of Concrete Compressive Strength

Equivalent reductions were observed in the ultimate capacity by approximately 16% and 23% for the 25 and 20 MPa values, respectively, relative to the reference value of model B1. In this study, the service load was the 70% of the ultimate load [30]. The deflection at this level clearly decreased by 28% and 31% for compressive strength values of 25 and 20 MPa, respectively, compared with the reference value of 30 MPa. The responses of the models with 25 and 20 MPa tended to exhibit similar behavior during the loading stages, which acted linearly until 70-80% of the ultimate load was reached, and exhibited curvature owing to plastic deformation of the C-channels prior to concrete crushing. The maximum deflection was 70 mm for both, having been increased by 55.55% more than the deflection of the model at 30 MPa, as illustrated in Table VII and presented in Figure 4.

TABLE VII. THE EFFECT OF THE COMPRESSIVE STRENGTH

f''c (MPa)	Max load (kN)	Reduction in max. load (%)	Def. at service load (mm)	Dec. Def. at service load (%)	Max def.	Inc. max. def. (%)
30	146	-	29	-	45	-
25	123	15.75	21	28	70	55.55
20	112	23.28	20	31	70	55.55

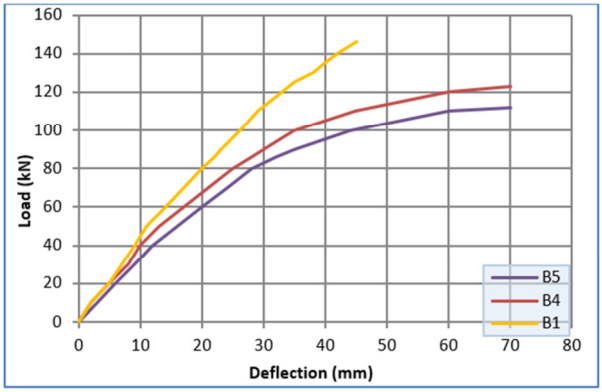

Fig. 4. Load-deflection curves of models with different compressive strengths.

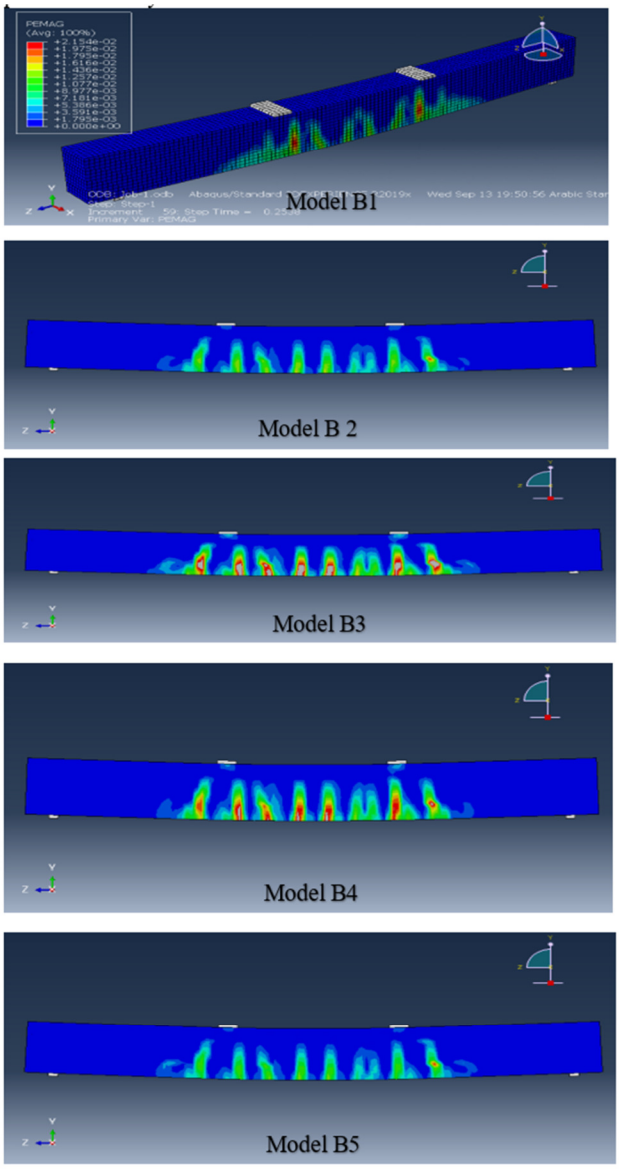

Fig. 5. Numerical crack patterns observed at failure for the models.

However, models with GFRP I-sections numerically showed the significant effects of the concrete compressive strength and GFRP reinforcement. The failure mode of all models was concrete crushing, which was controlled by the criteria of the flexural members. Figure 5 portrays the failure modes and crack patterns for these five models after releasing the analysis results from this parametric study.

VI. CONCLUSIONS

Based on the results of this parametric study, several important conclusions were drawn regarding the design and performance of composite beams with encased sections. The reinforcement ratio is a critical factor in the design process and must be considered when designing composite beams with encased sections. The performance of these beams exhibited linear behavior until concrete crushing became the controlling limit state. Notably, increasing the GFRP reinforcement ratio led to significant improvements in the load capacity, with gains of 29% and 41% observed for ratios of 0.85% and 1.2%, respectively. At the service stage, the deflection decreased by approximately 17.24% and 13.79%, whereas at the maximum stage, it increased by approximately 15% and 22% for models with GFRP reinforcement ratios of 0.85% and 1.2%, respectively.

The present study also revealed that a reduction in concrete compressive strength negatively impacted the structural behavior of the encased composite beams. Specifically, the ultimate capacity of the composite beams decreased by 16% and 23% for concrete compressive strengths of 25 MPa and 20 MPa, respectively, compared to the reference beams with a compressive strength of 30 MPa. Interestingly, at the service load, the deflection in the composite beams decreased by 28% and 31% when the compressive strength was reduced to 25 MPa and 20 MPa, respectively, relative to the reference beam with a 30 MPa compressive strength. It was observed that the models with 25 MPa and 20 MPa concrete strengths tended to exhibit similar behavior during various loading stages and behaved linearly until 70-80% of the maximum load.

REFERENCES

[1] Z. K. Al-Mamory and A. H. A. Al-Ahmed, "Behavior of steel fiber reinforced concrete beams with CFRP wrapped lap splice bars," *Structures*, vol. 44, pp. 1995–2011, Oct. 2022, https://doi.org/10.1016/j.istruc.2022.08.096.

[2] A. A. Abbood, N. Oukaili, A. A. Allawi, and G. Wardeh, "Strength and Deformation of Concrete-Encased Grouting-Filled Steel Tubes Columns Exposed to Monotonic Quasi-Static Loading Conditions," *Infrastructures*, vol. 9, no. 2, Feb. 2024, Art. no. 26, https://doi.org/10.3390/infrastructures9020026.

[3] A. A. Allawi, and S. I. Ali,, " Flexural behavior of composite GFRP pultruded I-section beams under static and impact loading," *Civil Engineering Journal*, vol. 6, no. 11, pp. 2143-2158, Nov. 2020, https://doi.org/10.28991/cej-2020-03091608.

[4] T. H. Ibrahim, A. A. Allawi, and A. El-Zohairy, "Impact Behavior of Composite Reinforced Concrete Beams with Pultruded I-GFRP Beam," *Materials*, vol. 15, no. 2, Jan. 2022, Art. no. 441, https://doi.org/10.3390/ma15020441.

[5] T. H. Ibrahim, A. A. Allawi, and A. El-Zohairy, "Experimental and FE analysis of composite RC beams with encased pultruded GFRP I-beam under static loads," *Advances in Structural Engineering*, vol. 26, no. 3, pp. 516–532, Feb. 2023, https://doi.org/10.1177/13694332221130795.

[6] T. H. Ibrahim, I. A. S. Alshaarbaf, A. A. Allawi, N. K. Oukaili, A. El-Zohairy, and A. I. Said, "Theoretical Analysis of Composite RC Beams with Pultruded GFRP Beams subjected to Impact Loading," *Engineering, Technology & Applied Science Research*, vol. 13, no. 6, pp. 12097–12107, Dec. 2023, https://doi.org/10.48084/etasr.6424.

[7] M. I. Ali, A. A. Allawi, and A. El-Zohairy, "Flexural Behavior of Pultruded GFRP–Concrete Composite Beams Strengthened with GFRP Stiffeners," *Fibers*, vol. 12, no. 1, Jan. 2024, Art. no. 7, https://doi.org/10.3390/fib12010007.

[8] E. M. Mahmood, A. A. Allawi, and A. El-Zohairy, "Flexural Performance of Encased Pultruded GFRP I-Beam with High Strength Concrete under Static Loading," *Materials*, vol. 15, no. 13, Jan. 2022, Art. no. 4519, https://doi.org/10.3390/ma15134519.

[9] M. Abdulkhaliq and A. H. Al-Ahmed, "The Flexural Behavior of One-Way Concrete Bubbled Slabs Reinforced by GFRP-Bars with Embedded Steel I-Sections," *Engineering, Technology & Applied Science Research*, vol. 14, no. 4, pp. 15860–15870, Aug. 2024, https://doi.org/10.48084/etasr.7680.

[10] A. H. A. Al-Ahmed, A. H. Al-Zuhairi, and A. M. Hasan, "Behavior of reinforced concrete tapered beams," *Structures*, vol. 37, pp. 1098–1118, Mar. 2022, https://doi.org/10.1016/j.istruc.2022.01.080.

[11] A. F. Hallawi and A. H. A. Al-Ahmed, "Enhancing the Behavior of One-Way Reinforced Concrete Slabs by Using Laced Reinforcement," *Civil Engineering Journal*, vol. 5, no. 3, pp. 718–728, Mar. 2019, https://doi.org/10.28991/cej-2019-03091282.

[12] M. R. Khalaf, A. H. A. Al-Ahmed, A. A. Allawi, and A. El-Zohairy, "Strengthening of Continuous Reinforced Concrete Deep Beams with Large Openings Using CFRP Strips," *Materials*, vol. 14, no. 11, Jan. 2021, Art. no. 3119, https://doi.org/10.3390/ma14113119.

[13] *ACI PRC-440.2-15: Guide for the Design and Construction of Externally Bonded FRP Systems for Strengthening Concrete Structures*. American Concrete Institute, 2015.

[14] *ACI CODE-440.11-22: Building Code Requirements for Structural Concrete Reinforced with Glass Fiber-Reinforced Polymer (GFRP) Bars—Code and Commentary*. American Concrete Institute, 2022.

[15] F. M. Bahlol and A. Al-Ahmed, "GFRP Encasing Efficiency on Enhancement Composite Beams under Static Loading," *Engineering, Technology & Applied Science Research*, vol. 14, no. 5, pp. 16897–16901, Oct. 2024, https://doi.org/10.48084/etasr.8064.

[16] M. A. E. Zareef, "An Experimental and Numerical Analysis of the Flexural Performance of Lightweight Concrete Beams reinforced with GFRP Bars," *Engineering, Technology & Applied Science Research*, vol. 13, no. 3, pp. 10776–10780, Jun. 2023, https://doi.org/10.48084/etasr.5871.

[17] F. M. Bahlol, A. M. Ibrahim, W. D. Salman, and H. A. Abdulhusain, "Effect of Steel Tube Thickness on Flexural Behavior of Concrete Composite Beams Using Different Section Shapes," *Diyala Journal of Engineering Sciences*, vol. 12, no. 4, pp. 41–49, Dec. 2019, https://doi.org/10.24237/djes.2019.12404.

[18] P. R. Johnson, *Composite Structures of Steel and Concrete: Beams, Slabs, Columns, and Frames for Buildings*. Wiley-Blackwell, 2004.

[19] A. M. Ibrahim, W. D. Salman, and F. M. Bahlol, "Flexural Behavior of Concrete Composite Beams with New Steel Tube Section and Different Shear Connectors," *Tikrit Journal of Engineering Sciences*, vol. 26, no. 1, pp. 51–61, Mar. 2019, https://doi.org/10.25130/tjes.26.1.07.

[20] M. N. S. Hadi and J. Youssef, "Experimental Investigation of GFRP-Reinforced and GFRP-Encased Square Concrete Specimens under Axial and Eccentric Load, and Four-Point Bending Test," *Journal of Composites for Construction*, vol. 20, no. 5, Oct. 2016, Art. no. 04016020, https://doi.org/10.1061/(ASCE)CC.1943-5614.0000675.

[21] "Abaqus." Dassault Systems, Available: https://www.3ds.com/products/simulia/abaqus.

[22] P. Kumar and A. Kumar, "Bending Analysis of Steel-Concrete Composite Beams with Porosity," *Engineering, Technology & Applied Science Research*, vol. 13, no. 4, pp. 11230–11234, Aug. 2023, https://doi.org/10.48084/etasr.6050.

[23] A. Hussein Ali Al-Ahmed, A. Al-Rumaithi, A. A. Allawi, and A. El-Zohairy, "Mesoscale analysis of Fiber-Reinforced concrete beams," *Engineering Structures*, vol. 266, Sep. 2022, Art. no. 114575, https://doi.org/10.1016/j.engstruct.2022.114575.

[24] M. Abdulkhaliq and A. H. Al-Ahmed, "Behavior of GFRP Reinforced-Concrete Bubbled One-Way Slabs by Encased Composite Steel I-Sections," *Engineering, Technology & Applied Science Research*, vol. 14, no. 5, pp. 16701–16712, Oct. 2024, https://doi.org/10.48084/etasr.8123.

[25] H. S. Ahmed, A. Allawi, and R. Hindi, "Experimental Investigation of Composite Circular Encased GFRP I-Section Concrete Columns under Different Load Conditions," *Engineering, Technology & Applied Science Research*, vol. 14, no. 5, pp. 17286–17293, Oct. 2024, https://doi.org/10.48084/etasr.8521.

[26] E. M. Mahmood, T. H. Ibrahim, A. A. Allawi, and A. El-Zohairy, "Experimental and Numerical Behavior of Encased Pultruded GFRP Beams under Elevated and Ambient Temperatures," *Fire*, vol. 6, no. 5, May 2023, Art. no. 212, https://doi.org/10.3390/fire6050212.

[27] N. K. Oukaili and A. A. Al-Asadi, "Analysis of Concrete Flexural Members Reinforced with Fibre Polymer," *Journal of Engineering*, vol. 16, no. 03, pp. 5569–5587, Sep. 2010, https://doi.org/10.31026/j.eng.2010.03.19.

[28] T. H. Ibrahim and A. A. Allawi, "The Response of Reinforced Concrete Composite Beams Reinforced with Pultruded GFRP to Repeated Loads," *Journal of Engineering*, vol. 29, no. 01, pp. 158–174, Jan. 2023, https://doi.org/10.31026/j.eng.2023.01.10.

[29] S. I. Ali and A. A. Allawi, "Effect of Web Stiffeners on The Flexural Behavior of Composite GFRP- Concrete Beam Under Impact Load," *Journal of Engineering*, vol. 27, no. 3, pp. 76–92, Feb. 2021, https://doi.org/10.31026/j.eng.2021.03.06.

[30] R. Park, "State-of-the Art Report: Ductility Evaluation from Laboratory and Analytical Testing," in *Proceedings of the 9th world conference on earthquake engineering*, Tokyo-Kyoto, Japan, 1988, vol. 8, pp. 605–616.